ARTICLE IN PRESS

Nature Communications

https://doi.org/10.1038/s41467-026-73580-5

Article in Press

Structural insights into *Arabidopsis thaliana* CTS-mediated fatty acid and hormone metabolism

Received: 25 October 2025

Accepted: 14 May 2026

Cite this article as: Zha, Z.-H., Peng, Y., Huang, D.-L. *et al.* Structural insights into *Arabidopsis thaliana* CTS-mediated fatty acid and hormone metabolism. *Nat Commun* (2026). https://doi.org/10.1038/s41467-026-73580-5

Zhi-Hui Zha, Yakun Peng, Dong-Liang Huang, Zhi-Peng Chen, Fang-Fang Wang, Bo-Rui Li, Bo Wang, Linfeng Sun, Ji-Shen Zheng, Shutang Tan, Cong-Zhao Zhou, Wen-Tao Hou & Yuxing Chen

We are providing an unedited version of this manuscript to give early access to its findings. Before final publication, the manuscript will undergo further editing. Please note there may be errors present which affect the content, and all legal disclaimers apply.

If this paper is publishing under a Transparent Peer Review model then Peer Review reports will publish with the final article.

ARTICLE IN PRESS

© The Author(s) 2026. **Open Access** This article is licensed under a Creative Commons Attribution-NonCommercial-NoDerivatives 4.0 International License, which permits any non-commercial use, sharing, distribution and reproduction in any medium or format, as long as you give appropriate credit to the original author(s) and the source, provide a link to the Creative Commons licence, and indicate if you modified the licensed material. You do not have permission under this licence to share adapted material derived from this article or parts of it. The images or other third party material in this article are included in the article's Creative Commons licence, unless indicated otherwise in a credit line to the material. If material is not included in the article's Creative Commons licence and your intended use is not permitted by statutory regulation or exceeds the permitted use, you will need to obtain permission directly from the copyright holder. To view a copy of this licence, visit http://creativecommons.org/licenses/by-nc-nd/4.0/.

ARTICLE IN PRESS

Structural insights into *Arabidopsis thaliana* CTS-mediated fatty acid and hormone metabolism

Zhi-Hui Zha[1, 2, 3, #], Yakun Peng[1, 2, 3, #], Dong-Liang Huang[4, 5, #], Zhi-Peng Chen[1, 2, 3], Fang-Fang Wang[1, 2, 3], Bo-Rui Li[1, 2, 3], Bo Wang[1, 2, 3], Linfeng Sun[1, 2, 3], Ji-Shen Zheng[1, 2, 3, *], Shutang Tan[1, 2, 3, *], Cong-Zhao Zhou[1, 2, 3, *], Wen-Tao Hou[1, 2, 3, *] & Yuxing Chen[1, 2, 3,*]

[1]Department of Endocrinology, The First Affiliated Hospital of USTC, Division of Life Sciences, University of Science and Technology of China, Hefei, China, [2]MOE Key Laboratory for Cellular Dynamics, Biomedical Sciences and Health Laboratory of Anhui Province, Hefei, China, [3]Hefei National Research Center for Physical Sciences at the Microscale, Hefei, China, [4]The Third Affiliated Hospital of Anhui Medical University, Institute of Clinical Pharmacology, School of Pharmacy, Anhui Medical University, Hefei, China, [5]Key Laboratory of Anti-inflammatory and Immune Medicine, Ministry of Education, Hefei, China.

# These authors contribute equally to this paper.

* Corresponding authors.

Email: cyxing@ustc.edu.cn; todvince@mail.ustc.edu.cn; zcz@ustc.edu.cn; sttan@ustc.edu.cn; jszheng@ustc.edu.cn

Abstract

In plants, peroxisomal β oxidation is essential for energy production, sugar metabolism and the regulation of hormonal signaling. The Arabidopsis *COMATOSE (CTS)* gene, which encodes the peroxisomal ATP-binding cassette transporter ABCD1 (also known as CTS or PAX1), mediates the import of various fatty acyls and hormones into peroxisomes for β oxidation. Although physiological evidence has demonstrated that defects in CTS impair plant development and growth, the underlying molecular mechanisms remain poorly understood. In this study, biochemical assays confirm that CTS transports a broad range of fatty acyl-CoAs, as well as indole-3-butyric acid (IBA), an auxin and precursor to indole-3-aceditc acid, and auxin herbicide 2,4-dichlorophenoxy butyric acid (2,4-DB). We further

ARTICLE IN PRESS

solve five cryo-EM structures of CTS: the apo form, ATP-bound, and three substrate-bound states (C12:0-, IBA- and 2,4-DB-CoA) at near-atom resolutions. These structures reveal that CTS binds a single substrate molecule in a characteristic U-shaped conformation. Moreover, physiological studies using point mutations of key substrate-binding residues identify critical residues essential for its function. Our findings reveal the molecular principles by which CTS integrates lipid metabolism, hormone regulation, and xenobiotic activation throughout the plant life cycle, as well as underscore its potential as a target for crop improvement and herbicide development.

Introdution

β oxidation is a crucial catabolic process that generates energy by breaking down fatty acid molecules for the growth of eukaryotic cells[1,2]. In plant cells, β oxidation is executed in peroxisomes, providing not only energy but also carbon skeletons for various biosynthetic processes, as well as hormones that regulate the seed germination, root development and responses to environmental stress[3].

Previous studies have shown that mutations in the peroxisomal ABC transporter COMATOSE (CTS, also known as AtABCD1, PXA1, PED3 or ACN2) from *Arabidopsis thaliana* lead to high levels of acyl-CoA accumulation due to a defect in the conversion of stored lipids to sucrose, which results in the failure of seedling establishment[4,5]. A subsequent study in which CTS was expressed in pxa1Δpxa2Δ (CTS ortholog) mutant yeast strains revealed that CTS enables the oxidation of saturated and unsaturated CoA-esterized fatty acids varying in length from C16 to C24[6]. Moreover, the *cts* mutants possess a reduced content of soluble carbohydrates converted from acetate, suggesting that CTS also participates in the metabolism of short-chain fatty acids[7]. Together, these findings indicate that CTS facilitates the import of a broad spectrum of fatty acids—including both long-chain and short-chain substrates—into peroxisomes thereby playing a central role in β oxidation. The

ARTICLE IN PRESS

essential contribution of CTS to this pathway has been further supported by studies showing that its mutants exhibit impairments in seedling development[4,5,8], stomal opening[9], starvation survival[10], etc., in *A. thaliana*.

Moreover, multiple alleles of *cts* were identified for resistance against the auxin indole-3-butyric acid (IBA) and the synthetic auxin herbicide 2,4-dichlorophenoxy butyric acid (2,4-DB)[11]. In peroxisomes, IBA and 2,4-DB are converted via β oxidation into indole-3-acetic acid (IAA)[12] and 2,4-dichlorophenoxyacetic acid (2,4-D)[13], respectively. As a major auxin, IAA regulates multiple stages of plant growth and development, such as cell division, cell expansion, cell differentiation and various tropic responses[14]. As a selective herbicide, 2,4-DB is specifically applied to control a broad spectrum of annual and perennial broad-leaved dicotyledonous weeds[15]. CTS loss-of-function leads to auxin-related defects in lateral root formation or delayed filament extension and flowering[8,16]. In addition, CTS was proposed to transport 12-oxo-phytodienoic acid (OPDA)[17], a major precursor of the hormone jasmonic acid (JA) in response to the mechanical, herbivorous or insect-induced damage and pathogenic infections of plants[18].

From the structural point of view, CTS is classified into the ATP-binding cassette (ABC) transporter ABCD subfamily that mediates the transport of substrates from the cytosol to the peroxisome[19-21]. Different from the human ABCD transporters, namely ABCD1, ABCD2 and ABCD3, which are half-transporters composed of two identical subunits[22-28], CTS is a full transporter containing two nucleotide-binding domains (NBDs) and two transmembrane domains (TMDs) in a single polypeptide[29]. As a ortholog of ABCD localize in the peroxisome membrane of plant cells, CTS was proposed to transport various substrates, covering the broad spectrum of human ABCD1/2/3 substrates; however, its structural information and molecular mechanism remain unclear.

ARTICLE IN PRESS

Here we present five structures of *A. thaliana* CTS determined via single-particle cryogenic electron microscopy (cryo-EM): the apo-form and ATP-bound structures at 3.2 Å and three structures in complex with various CoA-conjugated substrates, namely, C12:0-, IBA-, 2,4-DB-CoA at 3.4, 3.2, and 3.5 Å, respectively. Combined with site-directed mutagenesis and substrate-stimulated ATPase activity assays, our data provide biochemical evidence regarding a broad spectrum of substrates with a shared binding pattern. In addition, transgenic analysis of *cts* point mutations highlights its functional diversity. These results not only demonstrate the important roles of CTS in lipid and hormone metabolism in plants but also have the potential to guide crop improvement and the development of selective herbicides.

Results

Biochemical characterization and structure determination of CTS

We overexpressed full-length CTS in HEK293F cells and purified the recombinant protein for biochemical assays (Supplementary Fig. 1a). CTS was extracted from the membrane with the detergent lauryl maltose neopentyl glycol (LMNG) plus cholesteryl hemisuccinate (CHS), and solvent exchange to glycol-diosgenin (GDN) was performed during purification. The purified wild-type CTS protein (WT) displayed ATPase activity of K_m and V_{max} values at 2.26 mM and 35.96 mol Pi min^{-1} mol^{-1} protein, respectively (Fig. 1a). CTS has a degenerated catalytic site in NBD2; hence, its ATPase activity is solely contributed by the consensus site Glu607 in NBD1 (Supplementary Fig. 1b). Therefore, a variant of CTS generated by replacing Glu607 with Gln (E607Q) in NBD1 could completely abolish ATP hydrolysis activity (Fig. 1a).

We first investigated substrate-stimulated ATPase activity upon the addition of various fatty acyl-CoAs (Supplementary Fig 2c), and found that all fatty acyl-CoAs varying in the acyl chain length from C2 to C26 can significantly stimulate the

ARTICLE IN PRESS

activity of CTS (Fig. 1b). Notably, the medium- and long-chain fatty acids, such as C8:0-, C12:0- and C16:0-CoA, exhibited a greater stimulatory effect. Comparably, non-CoA-esterized substrates, either fatty acids or hormones, showed no stimulatory effect (Supplementary Fig 2a and 2b). Therefore, we synthesized two conjugated hormone precursor substrates, IBA-CoA and 2,4-DB-CoA, according to a previously described method[30,31]. We were able to obtain an overall yield of more than 70.0% for both products (Supplementary Fig. 3), which exhibit the substrate-stimulated ATPase activity comparable to that of C12:0-CoA (Fig. 1c). The half-maximal effective concentration (EC_{50}) values of C12:0-, IBA- and 2,4-DB-CoA were 0.26, 0.24 and 0.64 μM, respectively, and the V_{max} values were 124.6, 69.2 and 115.4 mol Pi min^{-1} mol^{-1} protein, respectively (Fig. 1c). These results not only confirmed that fatty acyl-CoAs are substrates of CTS but also demonstrated that the CoA-conjugated hormone precursors IBA-CoA and 2,4-DB-CoA are also substrates of CTS. In addition, these assays also indicated that our protein samples are in a physiologically relevant state.

However, the relatively low yield of CTS proteins has hindered further structural studies. Guided by our previous studies on human ABCD1 and ABCD3[22,27], we constructed a chimeric version of CTS (chCTS), in which the N-terminal 79 residues of CTS were replaced with the corresponding N-terminal 64-residue signal peptide of *Caenorhabditis elegans* PMP-4, that guides subcellular location to the peroxisome membrane[32]. The expression level of chCTS was indeed increased to ~2.2-fold that of CTS (Supplementary Fig. 1c). Biochemical assays revealed that chCTS behaves similarly to CTS (Fig. 1b). We further reconstituted the detergent-solubilized chCTS into lipid nanodiscs to compare its activity (Supplementary Fig. 4a), which displayed ATPase activity of K_m and V_{max} values at 2.19 mM and 27.20 mol Pi min^{-1} mol^{-1} protein (Supplementary Fig. 4b), respectively. The chCTS in nanodiscs also presented substrate-stimulated ATPase activity upon

ARTICLE IN PRESS

the addition of various fatty acyl-CoAs (Supplementary Fig. 4c). We also applied surface plasmon resonance (SPR) experiments with chCTS in nanodiscs and revealed that chCTS possesses an equilibrium dissociation constant (K_d) of 14 μM, 166 μM and 111 μM toward C12:0-CoA, IBA-CoA and 2,4-DB-CoA (Supplementary Fig. 4d-4f), respectively. These results indicated that the detergent-solubilized protein samples behave similarly with those in lipidic systems such as nanodiscs. In addition, the replacement of the N-terminus of CTS does not alter its interaction with substrates. Eventually, chCTS of higher yield enabled us to solve five cryo-EM structures (Fig. 1d): the apo-form structure at 3.2 Å (Supplementary Fig. 5), the C12:0-, IBA-, 2,4-DB-CoA-bound structures at 3.4, 3.2 and 3.5 Å (Supplementary Fig.6, 7 and 8), respectively, and the ATP-bound structure at 3.2 Å (Supplementary Fig. 9). Notably, the fused N-terminal segment of PMP-4, is missing in all these structures, most likely because of its high flexibility. Therefore, these structures indeed represent the core structure of *A. thaliana* CTS, and the term CTS is used to refer to all the structural information hereafter.

Overall structure of the apo-form CTS

The structure of apo-form CTS was solved at an overall resolution of 3.2 Å using 439,713 particles from the best class. In total, 1,178 residues were built into the EM density, except for some unstructured segments (Supplementary Fig. 5). Each TMD of CTS is composed of six transmembrane helices (TMs), which extend into the cytoplasm to form two divergent “wings” (Fig. 2a, c). Sharing a typical feature of type IV ABC transporters[33], helices TM4 and TM5 from TMD1, as well as the counterpart TM10 and TM11 from TMD2, are swapped to the opposite TMD (Fig. 2b). Two pairs of coupling helices (CH1 and CH2, CH3 and CH4) from the TMDs are embedded in the grooves on the NBDs, coupling the conformational changes between the TMDs and NBDs (Fig. 2a, c).

ARTICLE IN PRESS

The apo-form CTS adopts an inward-occluded conformation (Fig. 2a, b), similar to the previously reported apo-form structure of McjD[34], which is a type IV multidrug resistance protein from *Escherichia coli*. TM3-5 from TMD1 approaches TM9-11 from TMD2, resulting in closure of the translocation cavity, whereas the two NBDs remain separated from each other (Supplementary Fig. 10a). In contrast, the apo-form human ABCD1 (7RRA [http://doi.org/10.2210/pdb7RRA/pdb]) adopts an inward-facing conformation with an enlarged opening of the cavity and two completely separated NBDs (Fig. 2d)[24]. Superposition of the apo-form CTS with human ABCD1 yielded a root-mean-square deviation (RMSD) of 9.914 Å over 1034 aligned Cα atoms, revealing a significant conformational discrepancy between the two apo-form structures.

ARTICLE IN PRESS

C12:0-CoA binds to CTS with a distinct U-shaped conformation

Via incubating the CTS sample with 300 μM C12:0-CoA, we solved the C12:0-CoA-bound structure at a resolution of 3.4 Å (Fig. 1d), using 463,288 particles from the best class (Supplementary Fig. 6). The EM density of a C12:0-CoA molecule was clearly observed in the transmembrane cavity (Supplementary Fig. 11a). In general, the C12:0-CoA-bound CTS structure adopts an inward-facing conformation with a wider opening toward the cytosol compared to that in the apo-form structure (Fig. 3a).

Notably, previous reports of substrate-bound ABCD1[22,25] and ABCD3[27] structures revealed that two substrate molecules symmetrically bind to the translocation cavities (Supplementary Fig. 12). In contrast, CTS harbors only one molecule of C12:0-CoA, which adopts a U-shaped conformation (Fig. 3a), in an amphiphilic pocket in the membrane (Supplementary Fig 11b) mostly contributed by TMD2. The 3′-phospho-ADP moiety of CoA is buried in a hydrophilic pocket

ARTICLE IN PRESS

formed mainly by polar residues (Fig. 3b and Supplementary Fig. 12a). Specifically, the adenine ring is stabilized by Tyr346 and Thr350 from TM5, Asn784 from TM7 and Ser806 from TM8 via hydrogen bonds. The 3′-phosphate of ribose forms salt bridges with Lys345 from TM5 and with Arg773 from TM7, in addition to hydrogen bonds with Tyr346 from TM5, Ser777 from TM7, and Gln 1043 from TM12. The diphosphate group interacts with Arg1035 via a salt bridge, and with Ser1039 and Ser1042 from TM12 via two hydrogen bonds. The pantothenate and cysteamine moieties, which link the 3′-phospho-ADP and the fatty acyl chain, bend back at the hydrophobic arch formed by Phe134 from TM1 and Trp1007 from TM11, directing the fatty acyl chain toward the cytosol. The fatty acyl chain interacts with Thr385 from TM6 via a hydrogen bond. In addition, an extra density close to the fatty acyl chain could be fitted with a CHS molecule (Fig. 3a and Supplementary Fig. 11b), which should be the detergent introduced during purification.

Mutagenesis combined with activity assays further demonstrated that CTS variants with single mutation of residues in the C12:0-CoA-binding pocket, including Phe134, Lys345, Tyr346, Thr350, Arg773, Asn784, Ser806, Ser810, Trp1007 and Arg1035, presented significantly lower substrate-stimulated ATPase activities compared to the wild type (Fig. 3h). Notably, the two variants at Arg1035 and Ser810 have been observed to have defects in the degradation of seed-reserved lipids and subsequent postgerminative growth[4]. Of note, these mutants retained basal ATPase activities comparable to the wild type (Supplementary Fig. 11c). In contrast, mutation of the ATPase hydrolysis site, such as K487A of the Walker A motif and E607Q of the Walker B motif in NBD1 abolished either basal or substrate-stimulated ATPase activities totally (Supplementary Fig. 11c). These results further supported that the mutations mainly impact substrate interactions.

ARTICLE IN PRESS

IBA- and 2,4-DB-CoA also bind to CTS in the same pocket of C12:0-CoA

Our biochemical results revealed that two auxin precursors, IBA-CoA and 2,4-DB-CoA, both significantly stimulated the ATPase activity of CTS. To further confirm that IBA- and 2,4-DB-CoA are bona fide substrates of CTS, we incubated the protein samples with 300 μM synthesized IBA- and 2,4-DB-CoA, and eventually solved the IBA- and 2,4-DB-bound CTS structures at the resolutions of 3.2 and 3.5 Å (Fig. 1c and Supplementary Fig. 7 and 8), respectively. Superposition of these two structures against the C12:0-CoA-bound structure indicated that all three substrate-bound CTS structures have similar inward-facing conformations with a wider opening toward the cytosol (Supplementary Fig. 11d, in contrast to the apo-form CTS structure (Fig. 2a).

Both CoA-conjugated auxin precursors bind to the CTS with a U-shaped conformation similar to that of C12:0-CoA, especially the shared CoA moieties, which are stabilized by the same residues Lys345, Tyr346, Arg773 and Arg1035 (Fig. 3d, 3f and Supplementary Fig. 13b, 13c). Notably, the pantothenate of the CoA moiety, despite also folding back to the hydrophobic arch formed by TM1 and TM11, are stabilized by three additional hydrogen bonds with Arg382 from TM6 and with Ser1042 and Gln1043 from TM11 (Fig. 3d, 3f). Moreover, 2,4-DB-CoA interacts with Thr1006 from TM11 via one more hydrogen bond. IBA- and 2,4-DB-CoA stimulated ATPase activity assays of CTS variants with single mutations of the binding residues revealed a significant decrease in activity (Fig. 3h).

The three substrate-bound structures revealed a shared amphiphilic substrate-binding pocket in CTS. Specifically, the polar residues from TM5, TM7 and TM12 are responsible for fixing the CoA moiety, whereas the hydrophobic residues from TM5, TM6 and TM11 contribute to binding the acyl chain. Notably, the acyl chain reverts to accommodate itself to the shape of the hydrophobic patch formed by TM11 and TM12 (Fig. 3g). Despite we failed in synthesizing the CoA-conjugated OPDA,

ARTICLE IN PRESS

ARTICLE IN PRESS

the precursor of JA, we alternatively docked OPDA-CoA into the substrate-binding pocket (Supplementary Fig. 14b). Notably, the CHS molecule was removed from the substrate-bound complex structure, so that the longer acyl chain of OPDA-CoA could be well accommodated. The docking of a C26:0-CoA molecule into the pocket yielded consistent results (Supplementary Fig. 14b). The amphiphilic substrate-binding pocket of CTS possesses a large hydrophobic patch, which enables it to accommodate substrates with acyl chains of various lengths. It is consistent with our substrate-stimulated ATPase activity assays upon the addition of fatty acids of various length, as long as C26:0-CoA (Fig. 1b). In summary, the extensive polar and hydrophobic interactions ensure a binding pocket that recognizes the CoA moiety with high specificity while accommodating a variety of acyl chains from broad-spectrum fatty acids to hormones. Moreover, multiple-sequence alignment revealed that these substrate-binding residues are highly conserved in CTS homologs (Supplementary Fig. 15).

ARTICLE IN PRESS

ATP binding triggers the release of substrate from CTS

To better map the full transport cycle of CTS, we used the E607Q mutant of CTS with no detectable ATPase activity (Fig. 1a), to capture the ATP-bound conformation. Via adding both ATP and C12:0-CoA to the protein sample, we solved the ATP-bound structure at a resolution of 3.2 Å (Fig. 4a and Supplementary Fig. 9). Two extra densities, which are symmetrically sandwiched between the two NBDs, could be fitted with two ATP-Mg^{2+} molecules (Supplementary Fig.16a); however, no density for the C12:0-CoA molecule is found. The two ATP molecules bind to the cleft between the Walker A motif of one NBD and the ABC signature motif of the opposite NBD (Supplementary Fig. 16b), and the two NBDs are dimerized in a typical “head-to-tail” manner[35]. Accordingly, the conformational changes in NBDs are transferred to TMDs via two pairs of coupling helices and

eventually cause the ATP-bound CTS to exhibit an outward-occluded conformation (Fig. 4a), similar to the previously reported AMP-PNP-bound structure of McjD[36]. In this conformation, the translocation cavity is partly closed at the exit toward the peroxisomal matrix, suggesting a transient intermediate state after the extrusion of substrate.

Superposition of the ATP-bound and apo-form CTS structures yielded a root-mean-square deviation (RMSD) of 0.691 Å over 912 aligned Cα atoms (Fig. 4b). Upon ATP binding, the two NBDs approach towards each other by ~6 Å compared with the apo form (Supplementary Fig. 10a). Compared with the substrate-bound CTS structures, significant conformation changes occurred in the ATP-bound CTS structure. For example, the ATP-bound CTS has a narrower cavity than the C12:0-CoA-bound CTS (Fig. 4c), resulting from TM1-3, TM6 and TM8-10 tilting toward the central axis (Supplementary Fig. 10b). Moreover, the loop between NBD1 and TMD2, which is not observed in the apo form and substrate-bound forms, is folded into an α-helix in the ATP-bound structure (Fig. 4b and Supplementary Fig.16c and 16d). Sequence alignment revealed that the residues composing this helix is highly conserved (Supplementary Fig. 16e), reminiscent of the C-terminal helices of hABCD1, which was proposed to facilitate the dimerization of two separate NBDs[22].

The substrate-binding residues of CTS are crucial for the development and growth of *A. thaliana*

The above structures enabled us to assign a couple of residues essential for the transport of fatty acids and related hormones, indicating there should be more mutants leading to COMATOSE. Therefore, we generated a series of transgenic *Arabidopsis* plants that harbor various *cts* point mutations (Supplementary Fig.17). Imaging with confocal laser scanning microscopy revealed that these mutated versions of *CTS–Venus* are located in the peroxisome of root cells, similar to that of the wild-type CTS protein (Supplementary Fig. 17). A previous study showed that

ARTICLE IN PRESS

ARTICLE IN PRESS

CTS loss-of-function led to defective seed germination, due to impaired β oxidation of OPDA-CoA that over-accumulates in the seed[37]. Our substrate-bound structures of CTS revealed a dozen of binding residues, single mutations of which were applied to phenotype screening. Mutations of either Lys345, Tyr346, Arg382, Arg773 or Arg1035 displayed impaired seed germination on sucrose-free MS medium (Fig. 5a and Supplementary Fig. 18a), resembling the loss-of-function mutant (*cts*). In contrast, mutants F134A, T350A, N784A, S806A, T1006A and W1007A, showed normal germination comparable to the wild-type (Col-0) and the complementation line (CTS). Notably, the mutant S810N, which exhibited partial germination but defective seedling (Fig. 5a and Supplementary Fig. 18a), was able to develop into normal seedlings in the medium supplemented with sucrose (Fig. 5b and Supplementary Fig. 18b), whereas all other mutants possess a similar phenotype upon sucrose supplementation (Supplementary Fig. 18a and 18b).

The seeds of the five mutants that failed to germinate were punctured and cultivated in the MS medium with or without sucrose, as it was reported that exogenous sucrose could rescue seedling establishment in *cts* loss-of-function mutants after seed coat puncturing[38,39]. As shown in Fig. 5c and 5d, all five mutants displayed restored seedling growth only upon the addition of sucrose after seed coat puncturing. These findings demonstrated that Lys345, Tyr346, Arg382, Arg773 and Arg1035 are indeed physiologically essential for the elimination of OPDA-CoA and the conversion of fatty acyl-CoAs via β oxidation, whereas Ser810 is involved in fatty acyl-CoA transport.

It has been reported that peroxisomal conversion of IBA to IAA contributes to lateral root formation[40]. Upon treatment with IBA, the single-mutation transgenic lines K345A, Y346A, R382A, R773A, N784A, S810N and R1035A exhibited significantly reduced lateral root numbers, similar to the phenotype of the *cts* loss-of-function mutant (Fig. 5e and Supplementary Fig. 18c). Upon transport by CTS

ARTICLE IN PRESS

ARTICLE IN PRESS

and conversion to 2,4-D in the peroxisome, the auxin herbicide 2,4-DB inhibits primary root growth; thus, *cts* loss-of-function led to a reduced sensitivity to 2,4-D[41]. Compared to the wild type treated with 2,4-DB, all mutations K345A, Y346A, R382A, R773A, N784A, S810N, and R1035A showed the antagonistic effects, with significantly longer roots similar to *cts* (Fig. 5f and Supplementary Fig. 18d). Together, the residues Lys345, Tyr346, Arg382, Arg773 and Arg1035, which interact with the CoA moiety based on our substrate-bound structures, play important roles in substrate recognition and transport of OPDA-CoA, fatty acyl-CoAs, IBA-CoA, and 2,4-DB-CoA.

ARTICLE IN PRESS

Discussion

A broad range of CoA-thioesterified substrates are imported by the ABC transporters in the subfamily D from the cytosol into the peroxisomal matrix for β oxidation[28,29]. In human, three members of the ABCD family, ABCD1-3, which possess specific substrate preferences, transport various fatty acids into peroxisomes[28]. In contrast, the plants utilize only one ABCD transporter CTS to transport a broad spectrum of substrates into peroxisomes. Our present biochemical and structural analyses clearly showed that CTS can transport not only a variety of fatty acyl-CoAs, but also a couple of derived CoA-conjugated hormones.

Previous structural studies revealed that human ABCD1 and ABCD3 form homodimers[22,24-27]. In the case of ABCD1, two molecules of very long-chain fatty acids extend symmetrically across the transport cavity and bind to two TMDs[22] (Supplementary Fig. 12b and 12d). However, in the translocation pocket between two TMDs of CTS, we observed only one molecule of the substrate, adopting a U-shaped conformation. This relatively large pocket enables CTS to accommodate a variety of substrates with shorter or longer acyl chains. Moreover, the substrate-binding pocket could be divided into two parts: the hydrophilic patch is responsible

ARTICLE IN PRESS

for stabilizing the CoA moiety, whereas the hydrophobic patch contributes to fixing the acyl chain.

This amphiphilic substrate-binding pocket that could accommodate diverse fatty acids and derived hormones makes CTS a key player during multiple stages of plant development and growth (Fig. 6): At the stage of seed germination, OPDA should be transported into the peroxisomes via CTS; otherwise, accumulation of OPDA will lead to the defect of germination[37]. Afterwards, fatty acids are transported into peroxisomes for β oxidation to generate acetyl-CoA, which supplies the energy and carbon skeletons for the seedling of plants[42]. At the vegetative growth stage, CTS transports IBA into peroxisomes, facilitating the conversion of IBA to the bioactive auxin IAA, which can regulate auxin homeostasis and promote the development of lateral roots. Moreover, JA is necessary for pollen development or proper response to abiotic and biotic stresses; and its precursor OPDA should be transported into the peroxisome by CTS for further proceeding. In addition, the widely used auxin herbicide 2,4-D is also activated in the peroxisome from its precursor 2,4-DB, which is also a substrate of CTS.

Overall, this study bridges molecular transport mechanisms with complex physiological outcomes and offers avenues for crop improvement, herbicide design, and stress adaptation strategies, highlighting CTS as a versatile hub in plant metabolic regulation.

ARTICLE IN PRESS

Methods

Protein expression and purification

The codon-optimized full-length *CTS* gene encoding the CTS protein (UniProt ID: Q94FB9) and *C. elegans pmp-4* encoding the PMP4 protein (UniProt ID: O45730) were synthesized by Sangon Biotech Company. The chimeric *cts* gene, in which the N-terminal region of 79 amino acids (aa) was replaced by the N-terminal region of 64 aa from *pmp-4*, was generated via overlap PCR. The full-length *cts* gene and chimeric *cts* (termed chCTS hereafter) were subsequently cloned and inserted into a modified pCAG vector with an N-terminal FLAG tag (DYKDDDDK) via a ClonExpress® II One Step Cloning Kit (C113-02, Vazyme Biotech Co., Ltd.). Using homologous recombination of multiple fragments, site-directed mutagenesis was introduced by designing forward and reverse primers with point mutations and overlapping amplifying fragments.

For protein expression, HEK293F cells (R79007, Invitrogen) were cultured in SMM 293T-II medium (Sino Biological, Inc.) at 37°C, 130 rpm and 5% CO_2. The cells were transfected when the density reached 2.5-3.0 × 10^6 cells/mL. For cell transfection, 1.8-2 mg of plasmid was premixed with 4 mg of linear polyethylenimines (PEIs) (Polysciences, Inc.) with a MW of 25000 in 45 mL of fresh medium for 15 min, and then the mixture was added to 800 mL of HEK293F cells supplemented with 50 mL of fresh medium and incubated for another 15 min. The transfected cells were subsequently grown at 37°C for 12 h. Then, sodium butyrate (S102954-500 g, Aladdin) was added to a final concentration of 5 mM, followed by cultivation at 30°C for an additional 48 h before harvest. After centrifugation at 4000 x *g*for 5 min, the cell pellets were resuspended in lysis buffer containing 25 mM Tris-HCl (pH 7.5), 150 mM NaCl, 20% glycerol (v/v) and a 1× protease inhibitor cocktail (C0001, TargetMol). The suspension was frozen quickly in liquid nitrogen and stored at -80°C until further use.

ARTICLE IN PRESS

ARTICLE IN PRESS

All steps of the purification of chCTS for cryo-EM were performed at 4°C. To extract chCTS from the cell membrane, the cells were rotated gently for 2 h in 25 mM Tris-HCl (pH 7.5), 150 mM NaCl, 20% (v/v) glycerol, 5 mM ATP (Sangon Biotech), 5 mM $MgCl_2$, 1% (w/v) LMNG (Anatrace) and 0.1% (w/v) cholesteryl hemisuccinate (CHS, Anatrace). The insoluble material was removed via ultracentrifugation at 208,400 x *g* for 45 min (Beckman, Type 70 Ti) at 4°C. The supernatant was incubated with the anti-FLAG M2 affinity gel (Sigma–Aldrich) on ice for 1 h. The resin was then loaded onto the column and washed five times, each time with 5 mL of wash buffer containing 25 mM Tris-HCl (pH 7.5), 150 mM NaCl, 5% (v/v) glycerol, 0.5 mM ATP, 0.5 mM $MgCl_2$ and 0.02% (w/v) GDN (Anatrace). The target protein was further eluted with 6 mL of wash buffer supplemented with 200 μg/mL FLAG peptide. The protein eluate was concentrated via a 100-kDa MWCO Amicon Ultra centrifugal filter (Millipore) before being subjected to size-exclusion chromatography via a Superose 6 Increase 10/300 gel filtration column (GE Healthcare) equilibrated with 25 mM Tris-HCl (pH 7.5), 150 mM NaCl and 0.02% (w/v) GDN. The peak fractions containing chCTS were pooled and concentrated for further biochemical studies or cryo-EM experiments.

All the mutants of CTS and chCTS used for the biochemical assays and structure determination were expressed and purified in the same way as the wild-type chCTS protein.

For nanodiscs reconstitution, the concentrated chCTS proteins solubilized in 0.02% GDN were mixed with purified nanodisc scaffold protein MSP2N2 and brain polar extract phospholipid BPL (141101P, Avanti) at a molar ratio of 1:5:300. After incubating the mixture at 4 °C for 1 h, 0.8 g mL^{-1} of biobeads SM-2 (Bio-Rad) were added to the mixture, which was then gently rotated overnight at 14 °C to initiate reconstitution and remove detergent. The biobeads were removed the following day, and the collected chCTS in nanodiscs was applied to a Superdex 200 Increase 10/300

ARTICLE IN PRESS

column (GE Healthcare) pre-incubated with buffer containing 25 mM HEPES-NaOH pH 7.0 and 150 mM NaCl. Peak fractions were collected and concentrated for biochemical assays.

Chemical synthesis of IBA-CoA and 2,4-DB-CoA

Several CoA thioesters were synthesized via a previously described method involving the use of a mixed ethyl carbonate anhydride[30,31]. First, triethylamine (2.8 μL, 20 μmol) was incorporated into a mixture of the corresponding carboxylic acid (20 μmol), IBA (I6057, Macklin) or 2,4-DB (D-24756, HEOWNS) in a 5:2 CH_2Cl_2/THF (v/v, 0.92 mL) mixture under N_2 gas. The mixture was subsequently stirred for 10 min at 25°C. Next, 1.9 μL (20 μmol) of ethyl chloroformate was added in a single portion, and the mixture was stirred for 1 h at 25°C. The solvents were then evaporated under reduced pressure, after which the residue was dissolved in 0.4 mL of tert-butyl alcohol.

The synthetic steps for IAA-CoA differ slightly. First, triethylamine (2.8 μL, 20 μmol) was incorporated into a mixture of the corresponding carboxylic acid (20 μmol), IAA (I832115, Macklin) in anhydrous dioxane (0.5 mL) under N_2 gas. The mixture was subsequently stirred for 10 min at 25°C. Next, 1.9 μL (20 μmol) of ethyl chloroformate was added in a single portion, and the mixture was stirred for 5 min at 25°C. Then white solids rapidly formed in the solvent, which were removed by centrifugation.

Coenzyme A (A600320, Sangon Biotech) (14 mg, 20 μmol) was dissolved in 0.4 mL of 0.4 M $NaHCO_3$, added to the solution and stirred for 0.5 h at 25°C. Then, 1 M HCl was added to the solution to quench the reaction, and the pH was adjusted to 3–5. Finally, the solution was subjected to vacuum evaporation, after which the residue was dissolved in a water/CH_3CN (v/v, 4/1, 5 mL, pH 5-7) mixture and eluted from a C18 column (4.6×250 mm) using a gradient of 5% to 95% buffer B (Pure

ARTICLE IN PRESS

CH_3CN) in buffer A (Pure water) over 30 min to afford the product (IBA-COA, 2,4-DB-COA, or IAA-CoA) in a good yield (74.0%, 70.0%, or 68.0%) after lyophilization. The product was confirmed by ESI–MS and ^{1}H-NMR characterization. The synthesized IBA-CoA and 2,4-DB-CoA were subsequently dissolved in 25 mM Tris-HCl (pH 7.5) and 150 mM NaCl for ATPase activity assays and structure determination, respectively.

ATPase activity assays

The ATPase activities of wild-type CTS and all the mutants were measured via an ATPase colorimetric assay kit (Innova Biosciences) in 96-well plates at an $OD_{630\ nm}$[43]. To measure the ATPase activities of CTS against different substrates, including C8:0 (C2875, Sigma-Aldrich), C12:0 (W261408, Sigma–Aldrich), IBA, 2,4-DB, IAA, C2:0-CoA (A2181, Sigma-Aldrich), C4:0-CoA (B130756, aladdin), C8:0-CoA (870708P, Sigma-Aldrich), C12:0-CoA (L2659, Sigma-Aldrich), C16:0-CoA (870716P, Sigma-Aldrich), (4ME) C16:0-CoA (870742P, Sigma–Aldrich), C22:0-CoA (870722P, Sigma-Aldrich), C24:0-CoA (870724P, Sigma-Aldrich), C26:0-CoA (870726P, Sigma-Aldrich), IBA-CoA, 2,4-DB-CoA and IAA-CoA or varying ATP (A26209, Sigma–Aldrich) concentrations, protein at a final concentration of 0.05 μM was added to the reaction buffer containing 50 mM Tris-HCl, pH 7.5, 50 mM KCl, 0.02% (w/v) GDN, and 2 mM $MgCl_2$. Notably, chCTS in nanodiscs at a final concentration of 0.05 μM was added to the buffer without 0.02% (w/v) GDN. Then, C12:0, IBA, 2,4-DB, C12:0-CoA, IBA-CoA or 2,4-DB-CoA was diluted to different concentrations and added to the reaction mixture. The mixture was incubated on ice for 10 min. The reaction was started by the addition of ATP at a final concentration of 2 mM (for the ATPase activity assay of CTS against different substrates) or of varying ATP concentrations and incubated for 20 min at 37°C. The amount of released Pi was quantitatively measured with a SpectraMax iD5 Multi-

ARTICLE IN PRESS

Mode Microplate Reader (Molecular Devices) in 96-well plates at an optical density of 630 nm (OD_{630}). The data are presented as the means ± SDs of biological replicates from three independent assays (n = 3).

SPR experiments

All SPR experiments were performed on a Biacore 8000 instrument (Cytiva) at 25 °C in a buffer of 20 mM HEPES-NaOH pH 7.0, 150 mM NaCl and 0.05% Tween 20. The purified chCTS in lipid nanodiscs was covalently immobilized onto the series S CM5 sensor chips (Cytiva) by amine coupling chemistry. Different concentrations of C12:0-CoA, IBA-CoA or 2,4-DB-CoA in the running buffer were serially flowed over the chip surface with the immobilized protein and the blank for 1 min at a flowrate of 30 μL min^{-1}. The data were fitted with steady-state affinity binding model using Biacore Insight Evaluation software. The graphs were plotted using Origin 2023 software.

Cryo-EM sample preparation and data collection

Apo-form chCTS was concentrated to 6 mg/mL for cryo-EM sample preparation. After centrifugation at 12000 × g for 10 min, 3.5 μL of the protein sample was applied to glow-discharged Quantifoil R1.2/1.3 300-mesh Cu Holey Carbon Grids and plunged frozen in liquid ethane via a Vitrobot Mark IV (FEI) at 4°C and 100% humidity. The blot time was 3.5 s, and the blot force was 0. To prepare the complex sample, 300 μM C12:0-CoA, IBA-CoA or 2,4-DB-CoA dissolved in purification buffer was incubated with apo-form chCTS for 30 min at 4 °C before being passed through freezing grids. For the ATP-bound complex sample, the purified $chCTS^{E607Q}$ was mixed with 300 μM C12:0-CoA and 10 mM ATP-$MgCl_2$ and incubated for 30 min at 4 °C before being passed through freezing grids.

ARTICLE IN PRESS

ARTICLE IN PRESS

Cryo-EM images were recorded via an EPU under a 300 keV Titan Krios electron microscope (FEI), which is equipped with a K3 Summit direct electron detector (Gatan). All datasets were collected in superresolution mode at a nominal magnification of ×81,000, corresponding to a pixel size of 1.07 Å, with a defocus range from -2.2 μm to -1.5 μm. For apo-form chCTS, C12:0-CoA-bound chCTS and ATP-bound chCTS^{E607Q}, each stack containing 32 frames was exposed for 4.2 s with a total dose of 55 $e^-/Å^2$. For IBA-CoA-bound and 2,4-DB-CoA-bound chCTS, each stack containing 32 frames was exposed for 3.8 s with a total dose of 50 $e^-/Å^2$.

ARTICLE IN PRESS

Cryo-EM data processing

Dose-fractionated image stacks were applied to motion correction and contrast transfer function estimation, which were both performed in cryoSPARC 4.0.3[44]. Particles were automatically picked with a template picker and extracted for further 2D and 3D processing.

For apo-form chCTS, a total of 3,052,627 particles were automatically picked from 2,786 micrographs and then subjected to 2D classification. In total, 2,122,456 particles from the best classes were put into ab initio reconstruction and heterogeneous refinement. After multiround refinement, 439,713 particles were further subjected to nonuniform refinement, yielding a reconstruction map at an average resolution of 3.2 Å.

For C12:0-CoA-bound chCTS, a total of 2,729,498 particles were automatically picked from 2,931 micrographs and then subjected to 2D classification. In total, 1,602,492 particles from the best classes were put into ab initio reconstruction and heterogeneous refinement. After nonuniform refinement, 463,288 particles were further subjected to nonuniform refinement, yielding a reconstruction map at an average resolution of 3.4 Å.

ARTICLE IN PRESS

For IBA-CoA-bound chCTS, a total of 2,954,711 particles were automatically picked from 2,524 micrographs and then subjected to 2D classification. In total, 1,164,878 particles from the best classes were put into ab initio reconstruction and heterogeneous refinement. After multiround refinement, 353,872 particles were further subjected to nonuniform refinement, yielding a reconstruction map at an average resolution of 3.2 Å.

For 2,4-DB-CoA-bound chCTS, a total of 4,658,123 particles were automatically picked from 3,981 micrographs and then subjected to 2D classification. In total, 1,922,576 particles from the best classes were put into ab initio reconstruction and heterogeneous refinement. After multiround refinement, 572,683 particles were further subjected to nonuniform refinement, yielding a reconstruction map at an average resolution of 3.5 Å.

ARTICLE IN PRESS

Model building and refinement

The structural model of apo-form chCTS was built on the basis of an initial model predicted by AlphaFold2[45] and refined with secondary structure and geometry restraints automatically or manually via real-space refinement in PHENIX 1.20.1[46] or WinCoot 0.9.8.1[47]. Finally, residues Gly85-Gly427, Glu444-Asp664, Gln711-Gly1081, and Asp1092-Gln1334 of the apo form were built into the map. For C12:0-CoA-bound chCTS, residues Gly86-Gly427, Glu444-Asp664, and Gln711-Glu1337 were built and refined according to the structure model of apo-form chCTS with a C12:0-CoA molecule and a CHS molecule manually built into the extra densities between TMD1 and TMD2. For IBA-CoA-bound chCTS, residues Gly86–Gly427, Glu444-Asp664, and Gln711–Glu1337 were built and refined according to the structural model of apo-form chCTS with an IBA-CoA molecule and a CHS molecule manually built into the extra densities between TMD1 and TMD2. For 2,4-DB-CoA-bound chCTS, residues Gly86-Asp428, Glu444-Asp664, and Gln711-

ARTICLE IN PRESS

Glu1337 were built and refined according to the structure model of apo-form chCTS with a 2,4-DB-CoA molecule and a CHS molecule manually built into the extra densities between TMD1 and TMD2. Owing to their relatively poor densities, the NBDs of substrate-bound chCTS were manually fitted onto the map via the NBD structure from ATP-bound chCTS^{E607Q} and were automatically refined in PHENIX 1.20.1[46]. For ATP-bound chCTS^{E607Q}, residues Gly85-Asp428, Ser443-Asp663, Asp680-Gly1081, and Asp1092-Gln1334 were built and refined according to the structure model of apo-form chCTS with ATP-Mg^{2+} fitted into prominent densities between two NBDs.

All the structures were validated with PHENIX 1.20.1[46] and MolProbity 4.02[48]. The model refinement and validation statistics are summarized in Supplementary Table 1. UCSF ChimeraX 1.7.1[49] and PyMOL2.6.2 (https://pymol.org) were used to prepare the structural figures. The protein sequences were aligned via Multalin (http://multalin.toulouse.inra.fr/multalin/), and the sequence alignment figures were generated via the ESPript 3 server (https://espript.ibcp.fr/).

Plant materials and growth conditions

All *Arabidopsis thaliana* materials used in this study were in the Col-0 background. The *pxa1-2*(SALK_019334), i.e. *cts* mutant was previously described[50] All seeds were surface sterilized with 75% alcohol and transferred to 1/2MS medium with 1% (w/v) sucrose and 0.8% plant agar (pH 5.8). After 2 days with 4℃ treatment, these seeds were moved into a plant growth chamber at 22 ℃ with a long-day photoperiod (16 h light/8 h dark) for 7 days. Afterwards, the germinating seedlings were transferred to the soil until the plants matured three months later. The point mutation vectors were transformed into *Agrobacterium tumefaciens* strain GV3101 by electroporation and then into *pxa1-2* mutant.

ARTICLE IN PRESS

ARTICLE IN PRESS

Phenotypic analysis and pharmacological treatments

For phenotyping of seedlings, seeds were grown on 1/2MS medium with or without sucrose, stratified at 4°C for 2 days, and moved to plant growth incubator at 22 °C. After 7 days, MS plates were imaged with a Sony A6000 camera with a macro lens to record germination status.

For pharmacological treatments, the seeds were punctured to ensure germination and sown on 1/2MS plates. After stratification for 2 days at 4 °C, moved to plant growth incubator for 3 days, the germinating seedlings were transferred to 1/2MS medium supplemented with 1 μM 2, 4-DB for 7 days, and then the primary root length was analyzed with ImageJ software. For IBA treatment, after stratification for 2 days at 4°C, moved to a plant growth incubator for 6 days, the germinating seedlings were transferred to 1/2MS medium supplemented with 5 μM IBA for 4 days, and then the number of lateral roots was measured.

ARTICLE IN PRESS

Fluorescence Colocalization Analysis

Transgenic lines expressing CTS-Venus and mCherry-PEX11e were genetically crossed. F1 progeny was identified through fluorescence screening. For imaging, 5-day-old seedlings were observed by laser-scanning microscopy (CLSM) through the Zeiss LSM980 equipped with a GaAsP detector. The manufacturer's default settings (smart mode) were used to image proteins tagged with Venus (excitation, 508 nm; emission, 524 nm) and mcherry (excitation, 561 nm; emission, 630 nm). All of the images were obtained at an 8-bit depth with 2× line averaging.

Data Availability

The cryo-EM density maps of five structures generated in this study have been deposited at the Electron Microscopy Data Bank under accession codes: EMD-65928 [https://www.ebi.ac.uk/pdbe/entry/emdb/EMD-65928] for apo-form CTS,

ARTICLE IN PRESS

EMD-65936 [https://www.ebi.ac.uk/pdbe/entry/emdb/EMD-65936] for C12:0-CoA-bound CTS, EMD-65943 [https://www.ebi.ac.uk/pdbe/entry/emdb/EMD-65943] for IBA-CoA-bound CTS, EMD-65951 [https://www.ebi.ac.uk/pdbe/entry/emdb/EMD-65951] for 2,4-DB-CoA-bound CTS, EMD-65937 [https://www.ebi.ac.uk/pdbe/entry/emdb/EMD-65937] for ATP-bound CTS, and the coordinates have been deposited at the Protein Data Bank under accession codes: 9WFG [http://doi.org/10.2210/pdb9WFG/pdb] for apo-form CTS, 9WFR [http://doi.org/10.2210/pdb9WFR/pdb] for C12:0-CoA-bound CTS, 9WG2 [http://doi.org/10.2210/pdb9WG2/pdb] for IBA-CoA-bound CTS, 9WG8 [http://doi.org/10.2210/pdb9WG8/pdb] for 2,4-DB-CoA-bound CTS, 9WFU [http://doi.org/10.2210/pdb9WFU/pdb] for ATP-bound CTS. The PDB code of the previously published structure used in this study is 7RRA [http://doi.org/10.2210/pdb7RRA/pdb]. Source Data are provided as a Source Date file.

ARTICLE IN PRESS

References

1 Houten, S. M., Violante, S., Ventura, F. V. & Wanders, R. J. A. The Biochemistry and Physiology of Mitochondrial Fatty Acid β-Oxidation and Its Genetic Disorders. *Annual Review of Physiology* **78**, 23-44 (2016). https://doi.org/https://doi.org/10.1146/annurev-physiol-021115-105045

2 Szrok-Jurga, S. *et al.* The Physiological and Pathological Role of Acyl-CoA Oxidation. *International Journal of Molecular Sciences* **24** (2023).

3 Kao, Y.-T., Gonzalez, K. L. & Bartel, B. Peroxisome Function, Biogenesis, and Dynamics in Plants. *Plant Physiology* **176**, 162-177 (2018). https://doi.org/10.1104/pp.17.01050

4 Hayashi, M. *et al.* Ped3p is a Peroxisomal ATP-Binding Cassette Transporter that might Supply Substrates for Fatty Acid β-Oxidation. *Plant and Cell Physiology* **43**, 1-11 (2002). https://doi.org/10.1093/pcp/pcf023

5 Footitt, S. *et al.* Control of germination and lipid mobilization by <i>COMATOSE</i>, the <i>Arabidopsis</i> homologue of human ALDP. *The EMBO Journal* **21**, 2912-2922-2922 (2002). https://doi.org/https://doi.org/10.1093/emboj/cdf300

6 Nyathi, Y. *et al.* The Arabidopsis Peroxisomal ABC Transporter, Comatose, Complements the Saccharomyces cerevisiae pxa1 pxa2Δ Mutant for Metabolism of Long-chain Fatty Acids and Exhibits Fatty Acyl-CoA-stimulated ATPase Activity*. *Journal of Biological Chemistry* **285**, 29892-29902 (2010).

ARTICLE IN PRESS

https://doi.org/https://doi.org/10.1074/jbc.M110.151225
7 Hooks, Mark A. *et al.* The Arabidopsis ALDP protein homologue COMATOSE is instrumental in peroxisomal acetate metabolism. *Biochemical Journal* **406**, 399-406 (2007). https://doi.org/10.1042/bj20070258
8 Zolman, B. K., Silva, I. D. & Bartel, B. The Arabidopsis pxa1 Mutant Is Defective in an ATP-Binding Cassette Transporter-Like Protein Required for Peroxisomal Fatty Acid β-Oxidation. *Plant Physiology* **127**, 1266-1278 (2001). https://doi.org/10.1104/pp.010550
9 McLachlan, Deirdre H. *et al.* The Breakdown of Stored Triacylglycerols Is Required during Light-Induced Stomatal Opening. *Current Biology* **26**, 707-712 (2016). https://doi.org/https://doi.org/10.1016/j.cub.2016.01.019
10 Kunz, H.-H. *et al.* The ABC Transporter PXA1 and Peroxisomal β-Oxidation Are Vital for Metabolism in Mature Leaves of Arabidopsis during Extended Darkness *The Plant Cell* **21**, 2733-2749 (2009). https://doi.org/10.1105/tpc.108.064857
11 Dietrich, D. *et al.* Mutations in the Arabidopsis Peroxisomal ABC Transporter COMATOSE Allow Differentiation between Multiple Functions In Planta: Insights from an Allelic Series. *Molecular Biology of the Cell* **20**, 530-543 (2008). https://doi.org/10.1091/mbc.e08-07-0745
12 Strader, L. C., Culler, A. H., Cohen, J. D. & Bartel, B. Conversion of Endogenous Indole-3-Butyric Acid to Indole-3-Acetic Acid Drives Cell Expansion in Arabidopsis Seedlings *Plant Physiology* **153**, 1577-1586 (2010). https://doi.org/10.1104/pp.110.157461
13 Wain, R. L., Wightman, F. & Russell, E. J. The growth-regulating activity of certain ω-substituted alkyl carboxylic acids in relation to their β-oxidation within the plant. *Proceedings of the Royal Society of London. Series B - Biological Sciences* **142**, 525-536 (1997). https://doi.org/10.1098/rspb.1954.0041
14 Du, M., Spalding, E. P. & Gray, W. M. Rapid Auxin-Mediated Cell Expansion. *Annual Review of Plant Biology* **71**, 379-402 (2020). https://doi.org/https://doi.org/10.1146/annurev-arplant-073019-025907
15 Charles, J. M. *et al.* Evaluation of the in vitro genetic toxicity of 4-(2,4-dichlorophenoxy)butyric acid. *Mutation Research/Genetic Toxicology and Environmental Mutagenesis* **472**, 75-83 (2000). https://doi.org/https://doi.org/10.1016/S1383-5718(00)00130-3
16 Footitt, S. *et al.* The COMATOSE ATP-Binding Cassette Transporter Is Required for Full Fertility in Arabidopsis. *Plant Physiology* **144**, 1467-1480 (2007). https://doi.org/10.1104/pp.107.099903
17 Theodoulou, F. L. *et al.* Jasmonic Acid Levels Are Reduced in COMATOSE ATP-Binding Cassette Transporter Mutants. Implications for Transport of Jasmonate Precursors into Peroxisomes. *Plant Physiology* **137**, 835-840 (2005). https://doi.org/10.1104/pp.105.059352
18 Wang, Y., Mostafa, S., Zeng, W. & Jin, B. Function and Mechanism of Jasmonic Acid in Plant Responses to Abiotic and Biotic Stresses. *International Journal of Molecular Sciences* **22** (2021).
19 van Roermund, C. W. T. *et al.* The human peroxisomal ABC half transporter ALDP functions as a homodimer and accepts acyl–CoA esters. *The FASEB Journal* **22**, 4201-4208 (2008). https://doi.org/https://doi.org/10.1096/fj.08-110866
20 van Roermund, C. W. T., Ijlst, L., Wagemans, T., Wanders, R. J. A. & Waterham, H. R. A role for the human peroxisomal half-transporter ABCD3 in the oxidation of dicarboxylic acids. *Biochimica et Biophysica Acta (BBA) - Molecular and Cell Biology of Lipids* **1841**, 563-568 (2014). https://doi.org/https://doi.org/10.1016/j.bbalip.2013.12.001
21 Theodoulou, F. L., Holdsworth, M. & Baker, A. Peroxisomal ABC transporters. *FEBS Letters* **580**, 1139-1155 (2006). https://doi.org/https://doi.org/10.1016/j.febslet.2005.12.095
22 Chen, Z.-P. *et al.* Structural basis of substrate recognition and translocation by human very long-chain fatty acid transporter ABCD1. *Nature Communications* **13** (2022). https://doi.org/10.1038/s41467-022-30974-5
23 Jia, Y. *et al.* Structural and functional insights of the human peroxisomal ABC transporter ALDP. *eLife* **11**, e75039 (2022). https://doi.org/10.7554/eLife.75039

ARTICLE IN PRESS

ARTICLE IN PRESS

24 Le, L. T. M., Thompson, J. R., Dang, P. X., Bhandari, J. & Alam, A. Structures of the human peroxisomal fatty acid transporter ABCD1 in a lipid environment. *Communications Biology* **5**, 7 (2022). https://doi.org/10.1038/s42003-021-02970-w

25 Wang, R., Qin, Y. & Li, X. Structural basis of acyl-CoA transport across the peroxisomal membrane by human ABCD1. *Cell Research* **32**, 214-217 (2022). https://doi.org/10.1038/s41422-021-00585-8

26 Xiong, C. *et al.* Structural insights into substrate recognition and translocation of human peroxisomal ABC transporter ALDP. *Signal Transduction and Targeted Therapy* **8**, 74 (2023). https://doi.org/10.1038/s41392-022-01280-9

27 Li, Y. *et al.* Structural insights into human ABCD3-mediated peroxisomal acyl-CoA translocation. *Cell Discovery* **10**, 92 (2024). https://doi.org/10.1038/s41421-024-00722-8

28 Kawaguchi, K. & Morita, M. ABC Transporter Subfamily D: Distinct Differences in Behavior between ABCD1–3 and ABCD4 in Subcellular Localization, Function, and Human Disease. *BioMed Research International* **2016**, 6786245 (2016). https://doi.org/https://doi.org/10.1155/2016/6786245

29 Theodoulou, Frederica L., Carrier, David J., Schaedler, Theresia A., Baldwin, Stephen A. & Baker, A. How to move an amphipathic molecule across a lipid bilayer: different mechanisms for different ABC transporters? *Biochemical Society Transactions* **44**, 774-782 (2016). https://doi.org/10.1042/BST20160040

30 Loncaric, C., Merriweather, E. & Walker, K. D. Profiling a Taxol Pathway 10β-Acetyltransferase: Assessment of the Specificity and the Production of Baccatin III by In Vivo Acetylation in E. coli. *Chemistry & Biology* **13**, 309-317 (2006). https://doi.org/https://doi.org/10.1016/j.chembiol.2006.01.006

31 Nevarez, D. M., Mengistu, Y. A., Nawarathne, I. N. & Walker, K. D. An N-Aroyltransferase of the BAHD Superfamily Has Broad Aroyl CoA Specificity in Vitro with Analogues of N-Dearoylpaclitaxel. *Journal of the American Chemical Society* **131**, 5994-6002 (2009). https://doi.org/10.1021/ja900545m

32 Lee, A. *et al.* Role of NH2-terminal hydrophobic motif in the subcellular localization of ATP-binding cassette protein subfamily D: Common features in eukaryotic organisms. *Biochemical and Biophysical Research Communications* **453**, 612-618 (2014). https://doi.org/https://doi.org/10.1016/j.bbrc.2014.09.133

33 Thomas, C. *et al.* Structural and functional diversity calls for a new classification of ABC transporters. *FEBS Letters* **594**, 3767-3775 (2020). https://doi.org/https://doi.org/10.1002/1873-3468.13935

34 Bountra, K. *et al.* Structural basis for antibacterial peptide self-immunity by the bacterial ABC transporter McjD. *The EMBO Journal* **36**, 3062-3079-3079 (2017). https://doi.org/https://doi.org/10.15252/embj.201797278

35 Thomas, C. & Tampé, R. Structural and Mechanistic Principles of ABC Transporters. *Annual Review of Biochemistry* **89**, 605-636 (2020). https://doi.org/https://doi.org/10.1146/annurev-biochem-011520-105201

36 Choudhury, H. G. *et al.* Structure of an antibacterial peptide ATP-binding cassette transporter in a novel outward occluded state. *Proceedings of the National Academy of Sciences* **111**, 9145-9150 (2014). https://doi.org/10.1073/pnas.1320506111

37 Dave, A. *et al.* 12-Oxo-Phytodienoic Acid Accumulation during Seed Development Represses Seed Germination in Arabidopsis *The Plant Cell* **23**, 583-599 (2011). https://doi.org/10.1105/tpc.110.081489

38 Russell, L., Larner, V., Kurup, S., Bougourd, S. & Holdsworth, M. The Arabidopsis COMATOSE locus regulates germination potential. *Development* **127**, 3759-3767 (2000). https://doi.org/10.1242/dev.127.17.3759

39 Pinfield-Wells, H. *et al.* Sucrose rescues seedling establishment but not germination of Arabidopsis mutants disrupted in peroxisomal fatty acid catabolism. *The Plant Journal* **43**, 861-872 (2005). https://doi.org/https://doi.org/10.1111/j.1365-313X.2005.02498.x

ARTICLE IN PRESS

40 Strader, L. C. *et al.* Multiple Facets of Arabidopsis Seedling Development Require Indole-3-Butyric Acid–Derived Auxin. *The Plant Cell* **23**, 984-999 (2011). https://doi.org/10.1105/tpc.111.083071
41 Hayashi, M., Toriyama, K., Kondo, M. & Nishimura, M. 2,4-Dichlorophenoxybutyric Acid–Resistant Mutants of Arabidopsis Have Defects in Glyoxysomal Fatty Acid β-Oxidation. *The Plant Cell* **10**, 183-195 (1998). https://doi.org/10.1105/tpc.10.2.183
42 Eastmond, P. J. & Graham, I. A. Re-examining the role of the glyoxylate cycle in oilseeds. *Trends in Plant Science* **6**, 72-78 (2001). https://doi.org/https://doi.org/10.1016/S1360-1385(00)01835-5
43 Vardakou, M., Salmon, M., Faraldos, J. A. & O'Maille, P. E. Comparative analysis and validation of the malachite green assay for the high throughput biochemical characterization of terpene synthases. *MethodsX* **1**, 187-196 (2014). https://doi.org/https://doi.org/10.1016/j.mex.2014.08.007
44 Punjani, A., Rubinstein, J. L., Fleet, D. J. & Brubaker, M. A. cryoSPARC: algorithms for rapid unsupervised cryo-EM structure determination. *Nature Methods* **14**, 290-296 (2017). https://doi.org/10.1038/nmeth.4169
45 Jumper, J. *et al.* Highly accurate protein structure prediction with AlphaFold. *Nature* **596**, 583-589 (2021). https://doi.org/10.1038/s41586-021-03819-2
46 Liebschner, D. *et al.* Macromolecular structure determination using X-rays, neutrons and electrons: recent developments in Phenix. *Biological Crystallography* **75**, 861-877 (2019).
47 Emsley, P. & Cowtan, K. Coot: model-building tools for molecular graphics. *Biological crystallography* **60**, 2126-2132 (2004).
48 Williams, C. J. *et al.* MolProbity: More and better reference data for improved all-atom structure validation. *Protein Science* **27**, 293-315 (2018). https://doi.org/https://doi.org/10.1002/pro.3330
49 Pettersen, E. F. *et al.* UCSF ChimeraX: Structure visualization for researchers, educators, and developers. *Protein Science* **30**, 70-82 (2021). https://doi.org/https://doi.org/10.1002/pro.3943
50 Fan, J., Yu, L. & Xu, C. A Central Role for Triacylglycerol in Membrane Lipid Breakdown, Fatty Acid β-Oxidation, and Plant Survival under Extended Darkness *Plant Physiology* **174**, 1517-1530 (2017). https://doi.org/10.1104/pp.17.00653

ARTICLE IN PRESS

Acknowledgment

We thank Dr. Yong-Xiang Gao at the Center for Integrative Imaging, University of Science and Technology of China during cryo-EM image acquisition. We thank Drs. Liwen Jiang (The Chinese University of Hong Kong), Jinbo Shen (Zhejiang A&F University), and Linhui Yu (Northwest A&F University) for published materials.

Funding

W.-T.H discloses support for the research of this work from the Fundamental Research Funds for the Central Universities (WK9100000031). Y.C discloses support for publication of this work from the Ministry of Science and Technology

ARTICLE IN PRESS

of China (2024YFA1306103). D.-L.H discloses support for the research of this work from the National Natural Science Foundation of China (22507002). S.-T.T discloses support for the research of this work from the National Natural Science Foundation of China (32321001and 32570366).

Author contributions

Z.-H.Z. and Y.C. conceptualized this study. C.-Z.Z, Y.C and L.-F.S supervised the project. Z.-H.Z, W.-T.H and S.-T.T designed all the experiments. Z.-H.Z. F-F. W and B W performed cloning. Z.-H.Z. performed expression, purification, ATPase activity assays, cryo-EM sample preparation, screening and cryo-EM data collection. Z.-H.Z, Z.-P.C and B.-R.L performed structure determination and model refinement. Y.-K.P performed cultivate plants. Z.-H.Z and Y.-K.P performed phenotypic analysis and pharmacological treatments. Y.-K.P performed plants microscopy and image acquisition. D.-L.H and J.-S.Z performed chemical synthesis of IBA-CoA, 2,4-DB-CoA and IAA-CoA. All authors contributed to data analysis. Z.-H.Z, W.-T.H., C.-Z.Z., and Y.C. wrote the manuscript.

ARTICLE IN PRESS

Declaration of interests

The authors declare no competing interests.

ARTICLE IN PRESS

Figure Legends

Fig. 1 Biochemical characterization and structure determination of CTS.

a. ATPase activities of the wild-type CTS (WT) and the E607Q mutant. The data points of WT activity were fitted with the Michaelis–Menten equation.

b. ATPase activities of CTS and chCTS in the presence of various acyl-CoAs at 5 μM. Each bar represents the average of three independent experiments (n = 3), and the error bars represent the means ± standard deviations (SDs). One-way ANOVA was used to compare the statistical significance of the differences in CTS and chCTS activity toward basal and alternative substrates. p values of <0.05, 0.01, and 0.001 are indicated with*, **, and ***, respectively.

c. The substrate-stimulated ATPase activity of CTS in the presence of C12:0, IBA, 2,4-DB, C12:0-CoA, IBA-CoA or 2,4-DB-CoA. The data points are fitted with the Hill equation. The average value of CTS ATPase activity without the addition of any substrates is shown as the control line.

All data points in (**a**) to (**c**) represent the means of independent experiments (n=3), and the error bars indicate the means±SDs.

d. Refined cryo-EM maps of five CTS structures. The unsharpened maps are displayed as outlines to show the positions of the detergent micelles. The cryo-EM maps were colored by UCSF ChimeraX 1.7 according to the local resolution estimated by cryoSPARC 4.0.

Source data are provided as a Source Data file.

Fig. 2 Overall structure of apo-form CTS.

a. Cartoon representation of the apo-form CTS. The TMD1&NBD1 module is colored light blue, and the TMD2&NBD2 module is colored light green. The apical peroxisome membrane is indicated by gray lines.

ARTICLE IN PRESS

ARTICLE IN PRESS

b. Top view of cartoon representation of the TMDs. The transmembrane helices (TMs) are sequentially numbered.

c. A topological diagram of CTS in the same color scheme shown in **(a)**. The terminal residues of each structural segment are labeled. The obscured parts of the structure are represented by dashed lines. The TMs and coupling helices (CHs) are sequentially numbered. The membrane plane is indicated by the gray rectangle.

d. Superposition of the apo-form CTS (light blue) against the apo-form human ABCD1 (hABCD1, gray; Protein Data Bank: 7RRA [http://doi.org/10.2210/pdb7RRA/pdb]). The TMs with conformational changes are labeled. The NBDs of CTS are indicated.

ARTICLE IN PRESS

Fig. 3 Structures of CTS bound to various substrates, and the substrate binding pockets.

a, **c**, **e**, Cartoon representations of the C12:0-CoA-bound (**a**), IBA-CoA-bound (**c**), and 2,4-DB-CoA-bound (**e**) CTS. The TMD1&NBD1 module is colored light blue, and the TMD2&NBD2 module is colored light green. The C12:0-, IBA-, 2,4-DB-CoA, and CHS molecules are shown as spheres in yellow, salmon, slate and gray, respectively. The apical peroxisome membrane is indicated by gray lines.

b, **d**, **f**, Close-up views of the C12:0- (**b**), IBA- (**d**), and 2,4-DB-CoA (**f**) binding pockets. C12:0-, IBA- and 2,4-DB-CoA are shown as sphere-stick in yellow, salmon and slate, respectively. Substrate-binding residues are shown as sticks and labeled. The hydrogen bonds and salt bridges are indicated by black dotted lines.

g. Superposition of C12:0-, IBA- and 2,4-DB-CoA from the structures, which are colored yellow, salmon and slate, respectively.

C12:0- (**h**), IBA- (**i**), 2,4-DB-CoA- (**j**) stimulated ATPase activities of WT and mutants harboring single-residue mutations in the substrate-binding pocket. Each

ARTICLE IN PRESS

bar represents the average of independent experiments (*n*=3), and the error bars represent the means ± SDs. One-way ANOVA was used to examine the statistical significance of differences between the WT and mutant strains. The *p* values of all the mutants are <0.05, 0.01, and 0.001 and are indicated with*, **, and ***, respectively. For **h**, *P*=0.0056 for S777A compared with WT. For **i**, *P*=0.0002, *P*=0.0103 and *P*=0.0072 for S777A, S1042A and Q1043A, respectively, compared with WT. Source data are provided as a Source Data file.

Fig. 4 Structure of the ATP-bound CTS

a. Cartoon representation of the ATP-bound CTS. ATP and Mg^{2+} are displayed as yellow sticks and green spheres, respectively. The TMD1&NBD1 module is colored light blue, and the TMD2&NBD2 module is colored light green. The apical peroxisome membrane is indicated by gray lines.

b. Superposition of the ATP-bound CTS (light blue) against the apo-form CTS (gray). The LH (linker helix) colored in orange is the linker Asp680-Ala696 between NBD1 and TMD2 in the ATP-bound CTS.

c. Superposition of the ATP-bound CTS (light blue) against the C12:0-CoA-bound CTS (yellow).

ARTICLE IN PRESS

Fig. 5. Transgenic analysis of *cts* point mutations highlights its functional diversity.

a, b, Primary root length of 7-day-old Col-0, *cts*, *pCTS::CTS-Venus* and *cts* point mutant transgenic lines grown on MS medium without (**a**) and with (**b**)sucrose. Data are mean ± SD. Scale bars, 1 cm.

ARTICLE IN PRESS

c, d, Representative images and primary root length of the punctured seeds of *cts*, and *cts* point mutant transgenic lines grown on MS medium with (**c**) or without (**d**) sucrose for 7 days. Data are mean ± SD. Scale bars, 1cm.

e, Number of lateral roots of 10-day-old Col-0, *cts,* p*CTS::CTS-Venus* and *cts* point mutant transgenic lines after transfer to MS medium supplemented with 5 μM IBA. Data are mean ± SD.

f, Primary root length of 10-day-old Col-0, *cts*, *pCTS::CTS-Venus* and *cts* point mutant transgenic lines after transfer to MS medium supplemented with 1 μM 2, 4-DB. Data are mean ± SD.

For **a**-**f**, each dot represents an individual plant and n values represent the number of seedlings measured. Significant difference was determined by one-way ANOVA with Dunnett's multiple comparison tests for mutants versus compared to CoI-0 (**a**, **b**, **e**, **f**) or *cts* (**c**, **d**). The *p* values of all the mutants are <0.05, 0.01, and 0.001 and are indicated with*, **, and ***, respectively. ns, not significant. For **a**, *P*=0.6370, *P*=0.258, *P*=0.3413 and *P*=0.0013 for CTS, F134A, N784A and S806A, respectively, compared with CoI-0. For **b**, *P*=0.9966, *P*=0.0001, *P*=0.0003, *P*=0.005, *P*=0.0002, *P*=0.0378, and *P*=0.9141 for CTS, F134A, T350A, N784A, S806A, S810N and W1007A, respectively, compared with CoI-0. For **c**, *P*=0.0012 for R1035A compared with *cts*. For **d**, *P*=0.3544 and *P*=0.0355 for K345A and R382A compared with *cts*. For **e**, *P*=0.035, *P*=0.034, *P*=0.4828 and *P*=0.077 for CTS, F134A, S806A and W1007A, respectively, compared with CoI-0. For **f**, *P*=0.527, *P*=0.9955, *P*=0.8281 and *P*=0.5407 for CTS, F134A, S806A andW1007A, respectively, compared with CoI-0. Source data are provided as a Source Data file.

Fig. 6. Schematic representation of the coordinating role of CTS in different phases of plant life through transporting diverse substrates.

ARTICLE IN PRESS

ARTICLE IN PRESS

CTS mediates the peroxisomal import of multiple CoA-conjugated fatty acids and derivatives, including OPDA-CoA, fatty acyl-CoAs (C18:0-CoA), IBA-CoA, and 2,4-DB-CoA, which are subsequently metabolized via β oxidation into signaling molecules such as jasmonic acid (JA), indole-3-acetic acid (IAA), and acetyl-CoA, or converted into herbicides (2,4-D). These metabolic products regulate key developmental processes, including seed germination, seedling establishment, lateral root growth, and pollen development, as well as herbicide metabolism.

Editorial Summary
Researchers report five cryo-EM structures of the Arabidopsis peroxisomal transporter CTS, revealing how it imports fatty acids, hormone precursors, and herbicides into peroxisomes for β oxidation.

Peer review information: *Nature Communications* thanks Markus Geisler, Angus Murphy, and the other, anonymous, reviewers for their contribution to the peer review of this work. A peer review file is available.

ARTICLE IN PRESS

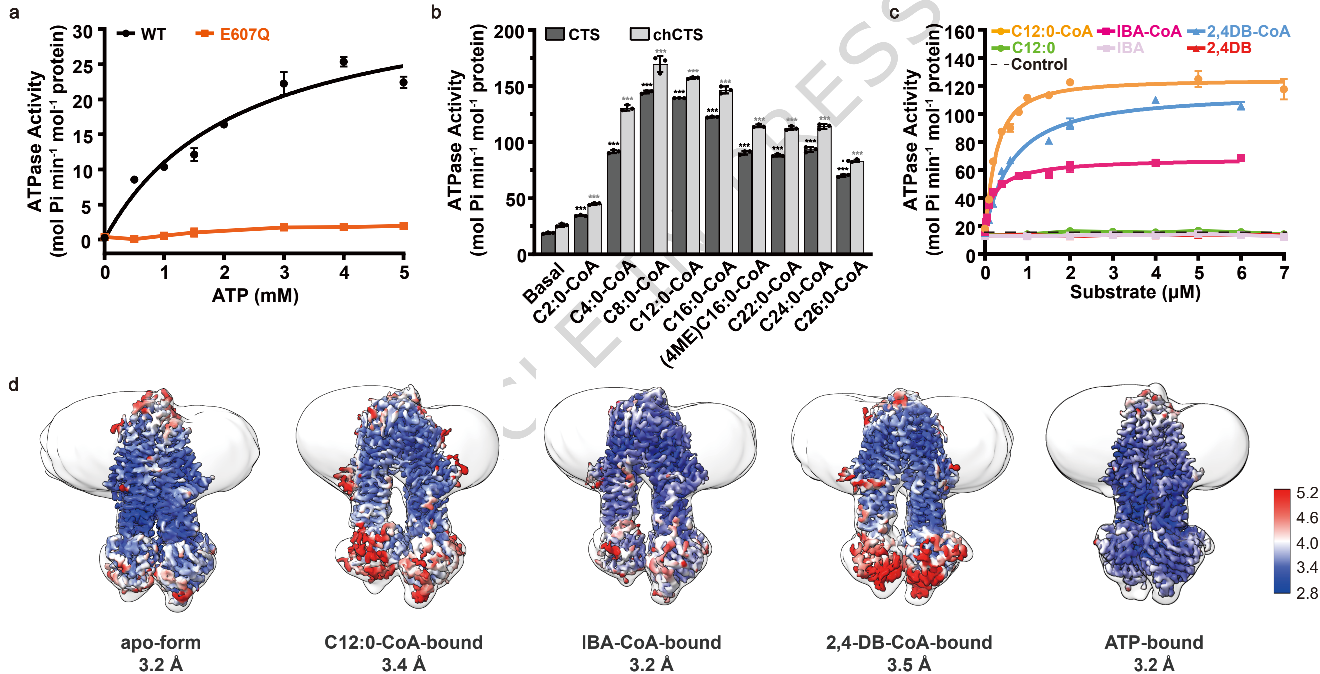
a
ATPase Activity (mol Pi min⁻¹ mol⁻¹ protein)
WT
E607Q
ATP (mM)
b
ATPase Activity (mol Pi min⁻¹ mol⁻¹ protein)
CTS
chCTS
Basal
C2:0-CoA
C4:0-CoA
C8:0-CoA
C12:0-CoA
C16:0-CoA
(4ME)C16:0-CoA
C22:0-CoA
C24:0-CoA
C26:0-CoA
c
ATPase Activity (mol Pi min⁻¹ mol⁻¹ protein)
C12:0-CoA
IBA-CoA
2,4DB-CoA
C12:0
IBA
2,4DB
Control
Substrate (μM)
d
apo-form
3.2 Å
C12:0-CoA-bound
3.4 Å
IBA-CoA-bound
3.2 Å
2,4-DB-CoA-bound
3.5 Å
ATP-bound
3.2 Å

ARTICLE IN PRESS

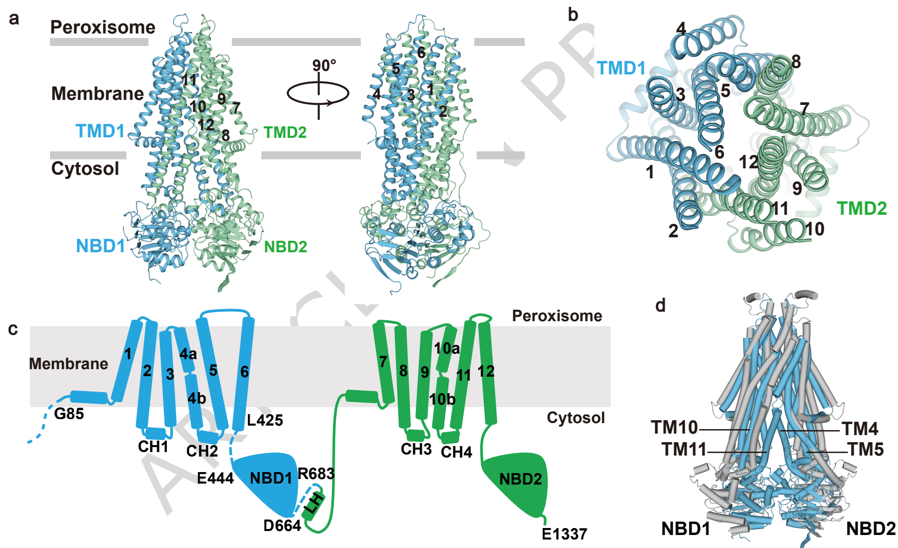

ARTICLE IN PRESS

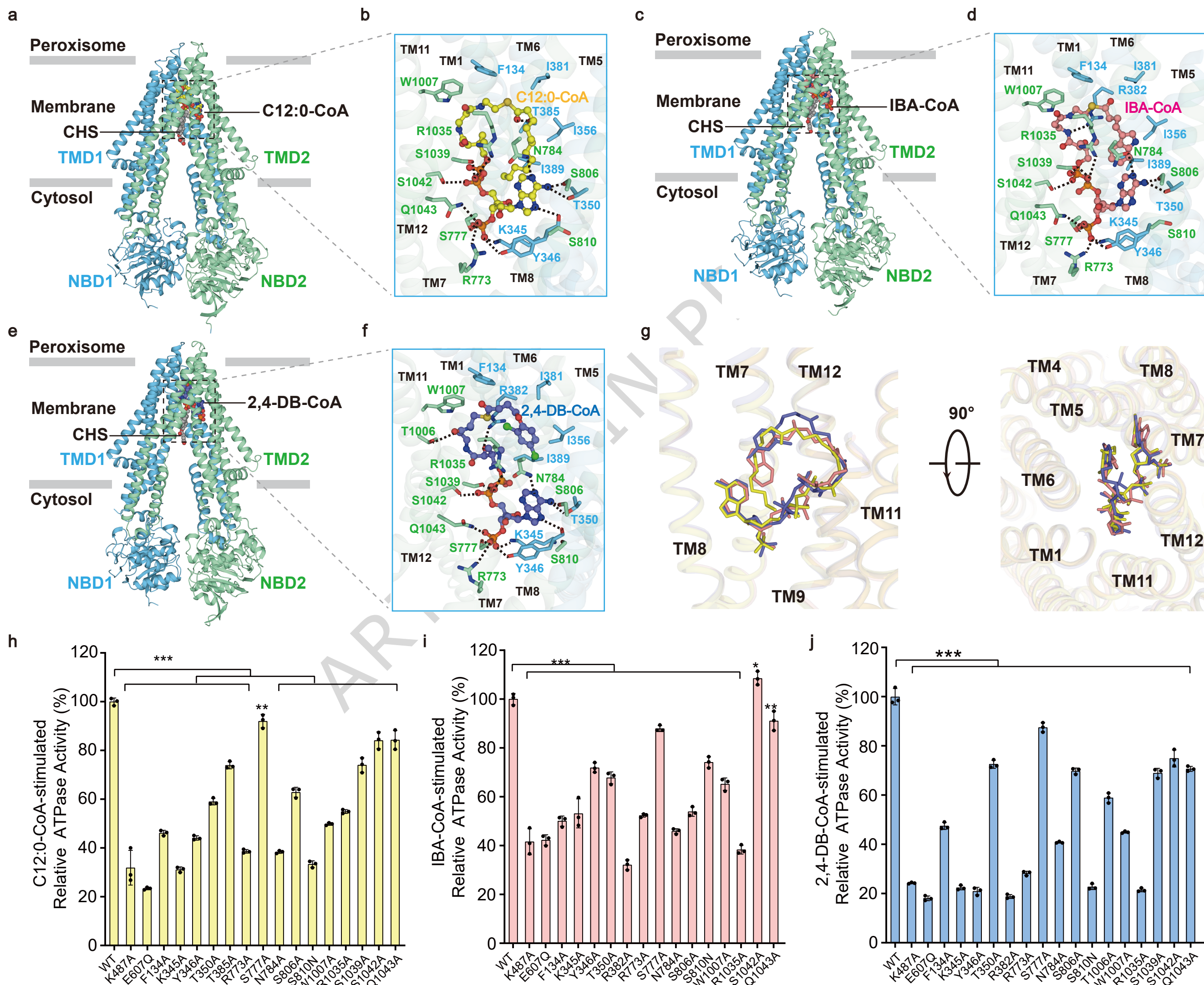

ARTICLE IN PRESS

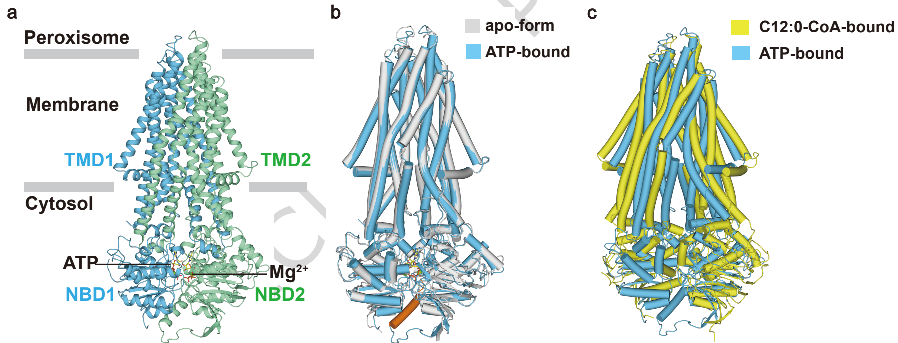

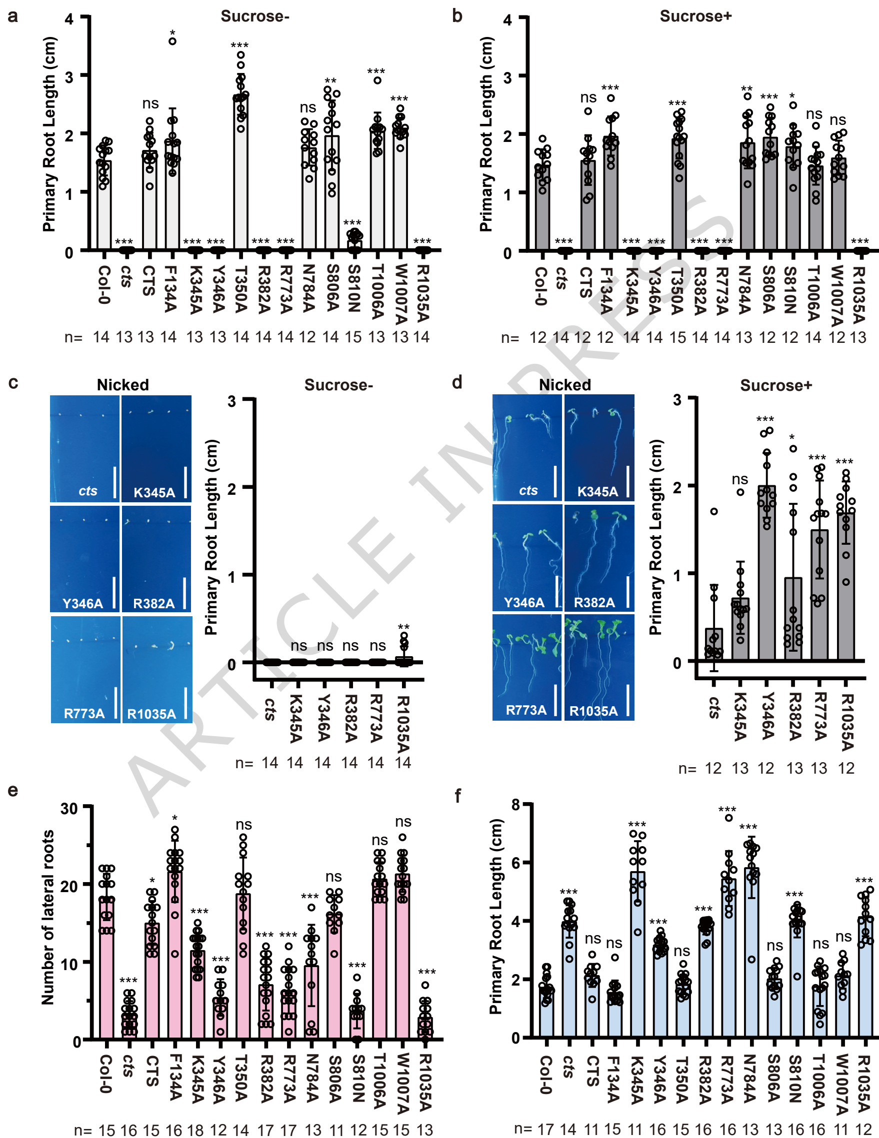

ARTICLE IN PRESS

ARTICLE IN PRESS